Exhaust gas fuel reforming of Diesel fuel by non-thermal arc discharge for NOx trap regeneration application

Alexandre Lebouvier, François Fresnet, Frédéric Fabry, Valérie Boch, Vandad-Julien Rohani, François Cauneau, Laurent Fulcheri

Exhaust gas fuel reforming of Diesel fuel by non-thermal arc discharge for NOx trap regeneration application

Alexandre Lebouvier[1,2], François Fresnet[2], Frédéric Fabry[1], Valérie Boch[2], Vandad Rohani[1], François Cauneau[1] and Laurent Fulcheri[1,]*

[1]Center for Energy and Processes, MINES ParisTech, Rue Claude Daunesse BP 207, 06904 Sophia Antipolis Cedex, France

[2]Technocentre Renault, Direction de la Recherche, des Etudes Avancées et des Matériaux DREAM/DTAA - Service 68240, 1 avenue du golf, 78288 Guyancourt Cedex, France

[*]To whom correspondence should be addressed. Phone: +33 (0)4 93 95 74 06. Fax: +33 (0)4 93 95 75 35. E-mail: laurent.fulcheri@mines-paristech.fr

Abstract

The present study is dedicated to the reforming of Diesel fuel with Diesel engine exhaust gas using a non-thermal plasma torch for NOx trap regeneration application. The plasma technology developed is based on a high voltage / low current non-thermal plasma torch. In the first part of the paper, experimental results on production of synthesis gas from Diesel fuel reforming with

Diesel engine exhaust gas are reported. In the second part of the paper, these experimental results are compared with a 1D multistage model with *n*-heptane as surrogate molecule for Diesel fuel. Two compositions of synthetic Diesel engine exhaust gas, corresponding to high and low engine loads respectively, have been studied. It has been demonstrated that the oxygen from CO_2 and H_2O hardly ever intervene in the exhaust gas Diesel fuel reforming. In the most favorable condition corresponding to higher O_2 rate, a production of 7.10^{-3} $mol.s^{-1}$ of syngas has been reached corresponding to an energy efficiency and a conversion rate of 40 % and 95 % respectively. The 1D multistage model shows good trends with experimental results despite an important correlation shift due to thermal losses which are not taken into account in the 1D model.

Keywords: Diesel fuel reforming, syngas production, non-thermal arc discharge, 1D model, plasma reformer, NOx trap regeneration application, Diesel engine after-treatment.

Introduction

Today in Europe, Diesel powered vehicles account for almost 50% of the passenger car market and up to 78% in France. Diesel engines offer several advantages over other internal combustion spark ignition engines due to their high energy efficiency and low level of CO_2 emissions. On the other hand, Diesel engines are generally characterized by higher nitrogen oxides (NOx) and Particulate Matter (PM) emissions than gasoline engines.

In Europe, Euro stage VI regulation for Diesel engines, coming into force in September 2014, set a 56 % reduction of NOx emissions compared to Euro stage V (80 $mg.km^{-1}$ vs. 180 $mg.km^{-1}$). This regulation forces car manufacturers to develop new efficient solutions. While current Three-

Way Catalysts (TWC) can efficiently lower NOx from spark ignition engines which operate under close to stoichiometric conditions, these technologies cannot be applied to Diesel vehicles since they are ineffective under oxidizing environment such as exhaust gas emitted from Diesel engines.

In Diesel engines, technologies based on NOx trap catalysts are one of the technological solutions under development to meet the further emission regulations. NOx trap technology, also called NOx Storage and Reduction (NSR), was first developed by Toyota in 1994[1]. This system operates with cycles composed of successive storage and regeneration modes. In storage mode, the NOx trap stores NOx emitted from the engine on a catalyst material generally based on Ba. Once full, the classical way to regenerate NOx trap catalysts consists in operating the engine under rich combustion conditions for a short while in order to produce reducing species in the exhaust gas[2], that will convert NOx into N_2. This method is not totally satisfying since it suffers from a significant drawback known as oil dilution problem. Oil dilution is the phenomenon characterized by Diesel fuel mixing together with engine oil. This phenomenon requires increasing change oil frequency.

To pass through oil dilution problem, it is possible to produce reducing species such as H_2 and CO by Diesel fuel reforming whose species will be used for NOx trap regeneration. When the NOx trap is full, a part of the Diesel engine exhaust gas is by-passed to the reformer and is mixed with a small amount of Diesel fuel, which provides the necessary species to regenerate the NOx trap catalyst. This method has the distinct advantage of not modifying engine conditions (*i.e.* avoiding short/rich combustion cycles) and avoiding oil dilution problem.

The catalytic exhaust gas fuel reforming of Diesel fuel is studied for several years by Megaritis *et al.* mainly for reformed exhaust gas recirculation (REGR) application[3-7]. The authors have demonstrated that REGR can reduce the exhaust emissions. They have investigated different hydrocarbons : natural gas[8], Diesel fuel[9,10], ultra low sulphur Diesel fuel (ULSD) and ultra-clean synthetic gas to liquid (GTL)[4,11], Biodiesel[6,10], Rapeseed methyl ester (RME)[12], bioethanol[8,13,14] and mixture[10,13] for Diesel engine[3-5,15] or HCCI engine[8,13,16,17]. The authors have focused their analysis on NOx and particulate matter (PM) reduction, the improvement of engine performances and the fuel economy[5,7,18]. The reformer was a nickel-free prototype catalyst, containing a low loading of precious metal promoted by metal oxides designed to promote all of the desired reactions: oxidation, steam reforming, dry reforming, and water gas shift reaction (WGSR) while at the same time inhibiting coke formation[4]. Some experiments have been realized for an aftertreatment unit, containing a HC-SCR catalyst[5,15,19]. The investigations have concerned essentially the EGR rate, the reactor inlet temperatures, the reformer configuration, the O/C ratio and λ. The aftertreatment unit performances was promoted by the presence of H_2 but inhibited by CO. Ref. 15 contains an exhaust gas composition very similar to our condition 2. 18 % of wet fraction of syngas has been achieved. The authors have tried to promote the H_2 production by WGSR and steam reforming for this application. High content of CO_2 has been also produced (+ 8 %) and almost no CH_4.

NOx can also be treated directly by plasma with DBD[20,21] or by Pulsed or DC Corona discharge[22,23] but the high content of oxygen in exhaust gas leads mainly to oxidize NO to NO_2[24,25]. Hence non-thermal plasmas alone achieve low NOx abatement. Recent researches on NOx removal have focused on hybrid process of non-thermal plasma (NTP) coupled with an

absorption process or a catalyst[26-28]. In plasma catalysis technology, the NTP is used as a pretreatment, to oxidize NO to NO_2, and facilitate the catalysis action.

For several years, intensive researches have been dedicated at CEP on reforming processes for fuel cell powering[29-32] using a non-thermal plasma torch. An alternative to the catalytic exhaust gas reforming of Diesel fuel method is presented in this paper and consists in using a NTP torch. Using a plasma torch as a reformer has been previously explored by several research teams[33]. Contrary to catalysts, plasma processes are non-sensitive to sulfur, low weight and low space device, and have short-transient time. The amount of oxygen in the plasma gas is a key point of this application, which directly affects the performance and the electric power needed. At engine high load, the oxygen becomes low in the exhaust gas.

Plasma reforming processes have been widely studied using different hydrocarbons with air (partial oxidation)[33-40], air and water mixture (autothermal reforming)[29,32,33] or CO_2 (dry reforming)[41-44] mostly with CH_4.

Some studies have been dedicated to the plasma assisted Diesel fuel reforming for NOx trap regeneration application by Bromberg *et al.* in association with ArvinMeritor[37-40] and more recently by Park *et al.*[45]. But all these techniques have used the partial oxidation of Diesel fuel with an additional air pump. The plasmatron GEN 2 of Bromberg *et al.* was one of the most advanced technology for POx of Diesel fuel. They have achieved up to 14.3 % and 8.2 % of CO and H_2[39] in cycling quickly the plasmatron every 3-5 seconds. The energy efficiency has attained 70 % for a deposited power up of 250 W[33]. 4.7 % of CO_2 have been produced, and also an important amount of CH_4 and C_2H_4 (2.6 and 2.4 % respectively). No soot has been observed.

To avoid the cost of an additional pump and injector, the plasma-assisted exhaust gas fuel reforming of Diesel fuel, with a high content of CO_2 and H_2O can be directly realized and is presented in this paper.

The partial oxidation reaction for a typical Diesel fuel at stoichiometry is:

$$C_{12.31}H_{22.49} + 6.15\,O_2 \Rightarrow 12.31\,CO + 11.25\,H_2\,;\ \Delta H = -1195\ kJ.mol^{-1}, \qquad (1)$$

The POx reaction is highly exothermic. At the contrary, the steam and dry reforming of Diesel fuel are significantly endothermic. These reactions are represented by the two equations hereafter:

$$C_{12.31}H_{22.49} + 12.31\,H_2O \Rightarrow 12.31\,CO + 23.55\,H_2\,;\ \Delta H = 1780\ kJ.mol^{-1}, \qquad (2)$$

$$C_{12.31}H_{22.49} + 12.31\,CO_2 \Rightarrow 24.62\,CO + 11.25\,H_2\,;\ \Delta H = 2887\ kJ.mol^{-1}, \qquad (3)$$

The high content of H_2O and CO_2 in the plasma gas (up to 9 % for each) lead to highly endothermic reactions, energetically unfavorable compared to partial oxidation of Diesel fuel, commonly studied.

The present study is dedicated to the reforming of Diesel fuel with Diesel engine exhaust gas by using a non-thermal plasma torch. After a presentation of the experimental set up, experimental results are presented and compared to thermodynamic and 1D multistage kinetic models. The effects of input current, O/C ratio, exhaust gas flow rate and cathode length versus energy efficiency and conversion rate are presented and discussed.

Experimental section

The experimental set-up developed in previous researches for fuel cell powering by gasoline, E85 and ethanol reforming[29,32] has been adapted to NOx trap regeneration application. Henceforth, it enables the injection and evaporation of Diesel fuel which has a higher boiling point than gasoline and ethanol. The experimental device also allows the synthetic reconstitution of Diesel engine exhaust gas composition corresponding to different operating regimes.

The experimental set-up is presented on figures 1 and 2. The plasma reactor is composed of two consecutive zones: a plasma zone and a post-discharge zone. The plasma zone is the part where the arc plasma really takes place. The post-discharge zone is a passive zone, located downstream the plasma zone where most of the reforming reactions ignited in the plasma zone continue to take place depending on their kinetic speed. The power supply is a resonant converter[46] controlled in current. The current can be precisely tuned in the range 0.22 – 0.66 A. The maximum voltage provided by the source is 15kV. A high voltage is applied to the tip electrode (anode as we work in inverse polarity) and the cylinder electrode (cathode) is grounded. The anode is 2.5 mm diameter composed mainly of Nickel. The cathode is a stainless steel cylinder with 8 mm inner diameter, 25 mm outer diameter and 75 mm or 100 mm long.

Three mass flow controllers supply a mixture of air, N_2 and CO_2 in the range 0-100 slpm (Brooks 5831 ES), 0-200 slpm (Air Liquide EL-FLOW) and 0-10 slpm (Bronkhorst F-201-CV) respectively. Two diaphragm metering pumps (KNF Stepdos FEM03 TT.18/RC) provide liquid water and Diesel fuel in the range 0-0.03 slpm. Water and Diesel fuel are then evaporated separately by two glow-plug systems to avoid steam cracking. The electrical consumption of the

plug flow systems is not considered in the energy efficiency calculations. The swirl injection of the reactants in the plasma torch is realized 10 mm before the tip electrode. The reactant temperature can be adjusted between ambient temperature and 600 K.

The post-discharge zone is 510 mm long. It is composed of a ceramic tube (Mullite C530) of 4 mm thickness and 22 mm inner diameter for thermal and electrical insulation. The ceramic is covered with a stainless steel tube of 1.6 mm thickness for mechanical purpose. The post-discharge zone is instrumented with 5 type K thermocouples, numbered from T1 to T5, located axially at 120, 180, 250, 330 and 460 mm from the cylindrical cathode output respectively. The thermocouples are located along the reactor axis except T1 and T2 thermocouples which have been off-centered to avoid thermal damage. T1 is located at the surface of the ceramic while T2 is located at 5.5 mm from the axis. After the post discharge output, a fraction of the reformate gas is deflected from the main flow and is rapidly cooled down before entering two analyzers placed in series. The reformate gas composition is first analyzed by a Rosemount NGA 2000 composed of two detectors: a Non-Dispersive InfraRed (NDIR) detector and a Thermal Conductivity Detector (TCD). This analyzer enables to continuously measure the dry molar fraction of H_2, CO, CO_2 and CH_4. The measurement is based on the assumption that the outlet dry gas only contains nitrogen and the four species above-mentioned. This assumption is verified with the second analyzer.

The second analyzer is a gas phase chromatograph Perichrom PR 2100. It is equipped of two independent analysis channels. The first channel is used to measure hydrogen with a molecular sieve 5Å column and a TCD. The carrier gas is nitrogen. The second channel is used to measure

CO, CO_2, CH_4 and C_2 hydrocarbons with a Poraplot U and a molecular sieve 5Å columns, a methanizer, a TCD, and a Flame Ionization detector (FID). The carrier gas is helium.

The electrical signals are analyzed by a HP 54615B oscilloscope (bandwidth of 500 MHz) with a high voltage probe Elditest GE3830 1:1000 (up to 30 kV) and hall effect current probe Chauvin Arnoux E3N (bandwidth of 100 kHz). The NDIR-TCD analyzer and thermocouples data are collected every second by a computer.

The fuel used is a commercial Diesel fuel. The table 1 reports the main characteristics of the fuel used for data analysis and of its surrogate molecule used for calculations.

Two operating conditions corresponding to different engine loads have been defined for this study: the exhaust gas composition of a Diesel engine for two fuel/air equivalence ratios (Φ) of 0.66 and 0.32 based on combustion equation for a Renault 2.0L 16v dCi turbocharged engine (M9R 842 1995cc). The equivalence ratio is defined by:

$$\phi = \frac{Q_{\text{fuel}}/Q_{air}}{Q_{\text{fuel}}/Q_{air}\big|_{stoich}} \ , \qquad (4)$$

where Q_{fuel} and Q_{air} refer to the molar flow rates of fuel and air respectively at engine intake. The first equivalence ratio corresponds to a high engine load and the second one to a low engine load. The gas composition for these both operating conditions is given in table 2.

The reactant mixture is represented in terms of O/C ratio. The O/C ratio stands for the molar ratio between oxygen atoms from air and carbon atoms from Diesel fuel and is defined in eq. 5. Note that oxygen coming from H_2O and CO_2 are not taken into account in this ratio.

$$\frac{O}{C} = \frac{2Q_{O_2}}{nQ_{C_nH_m}} = \frac{0.21Q_{air}}{12.31Q_{C_{12.31}H_{22.49}}} \quad , \qquad (5)$$

Q_i stands for the molar flow rate of species i and n the number of C atoms in the empirical formula of the fuel (C_nH_m). The stoichiometry of the partial oxidation reaction of Diesel fuel is O/C =1.

Plasma reformer performances are analyzed in terms of energy efficiency η and conversion rate χ, which are expressed as:

$$\eta = \frac{Q_{H_2} \times LHV_{H_2} + Q_{CO} \times LHV_{CO}}{Q_{fuel} \times LHV_{fuel} + W} \quad , \qquad (6)$$

$$\chi = \frac{Q_{CO} + \Delta Q_{CO_2} + Q_{CH_4}}{nQ_{fuel}} \quad , \qquad (7)$$

where LHV_i is the lower heating value of chemical species i and W is the electrical deposited power applied to the discharge. The conversion rate (eq. 4) accounts for the fuel transformation and is an indicator of the mass balance on carbon atoms. ΔQ_{CO2} corresponds to the difference between the output and input CO_2 molar flow rate. Only the main species (H_2, CO, CO_2, CH_4) was considered in these energy and mass balances. The other species $C_nH_mO_k$ formed were analyzed and quantified by GC. They were present in minor concentration when the conversion rate is high. In the results presented in this paper, the inlet temperature and working pressure have been set to 573 K and 0.1 MPa, respectively. For each measurement reported, the system is considered to be at the thermal steady state. A waiting time of 5 min is generally observed in order to allow the system to reach this equilibrium.

Modeling approaches

In both models presented below, *n*-heptane (C_7H_{16}) molecule has been chosen for calculations because it is a commonly used surrogate molecule for Diesel fuel. *n*-heptane has a cetane number of approximately 54[47] which is very similar to conventional Diesel fuel.

The thermodynamic equilibrium calculations are performed with EQUIL module from the CHEMKIN II package[48]. The algorithm is based on Gibbs free energy minimization. The modeling approach is detailed in ref. 6. This model assumes an infinite reactor, a perfect mix of species and a uniform application of the plasma power. Given the initial composition, the initial temperature and the reactor pressure, the initial enthalpy is evaluated. The initial temperature is 573 K and the pressure reactor is 0.1 MPa. The final mixture enthalpy is the sum of the initial enthalpy and the enthalpy coming from the plasma. The equilibrium composition and temperature are calculated from the final enthalpy.

The exhaust gas Diesel fuel reforming has also been simulated with a 1D kinetic model previously developed for gasoline reforming[31]. The model has been adapted for NOx trap regeneration application. Several *n*-heptane detailed mechanisms have been developed over the past two decades[49-56], widely for engine and propulsion devices. The calculations have been carried out using the *n*-heptane oxidation mechanism developed by Curran *et al.*[52,53]. It has been extensively validated in a wide range of temperature and pressure in different reactors, shock tubes and rapid compression machine experiments. This kinetic mechanism is composed of 160 species and 1540 reactions and can be applied to a wide range of conditions. This large mechanism makes it applicable to a wide range of conditions. Recent researches have focused on

reduced n-heptane mechanisms[56] based on the Curran *et al.* mechanism to integrate them in CFD models for example. This mechanism includes radicals, atoms and vibrationaly excited species but does not include ionized species. Most of kinetic mechanisms that have been developed (mainly for combustion issues) generally do not include all the ionized and excited species due to a lack of basic knowledge. Some chemical mechanisms including ionized species have been proposed for methane (CH_4)[58], propane (C_3H_8)[59] and *n*-butane (C_4H_{10})[60] with air. Because of the complexity of the involved mechanisms, no kinetic mechanism including charged species is available in the literature for higher hydrocarbons under reforming conditions. The plasma-assisted reforming process is far from these combustion processes due to low amount of present oxygen, and even further from the exhaust gas fuel reforming. However, the relevance of a combustion kinetic mechanism has been proven by Benilov and Naidis for low current arc discharge[61]. The mechanism has been first tested numerically in exhaust gas fuel reforming conditions in a plug flow reactor (PFR) for a very long time (~10^8 s) and then have been compared to a thermodynamic model based on T&TWinner[62] database. The results with the *n*-heptane kinetic mechanism from Curran *et al.* were consistent with the thermodynamic model.

It has been demonstrated that low current arc discharges are highly non-homogenous. This 1D multistage model, presented on figure 3, has been detailed in ref. 31. This model is based on the following assumptions: (i) the medium is adiabatic, (ii) only a fraction of reactants' inlet flow passes through the arc discharge, the remaining fraction passes near the arc and there is no mass transfer between the arc and the cold zone around the arc inside the reactor, (iii) these two fractions; *i.e.* cold and hot streams respectively, are perfectly and instantaneously mixed at the reactor exit. The arc is modeled by a Perfectly Stirred Reactor (PSR) where a homogenous input

power is applied. Experimentally, we can observe that the plasma radius is around 1 mm, the cathode radius being 4 mm. The assumption made is that the fraction of the gas that passes through the arc is equal to the ratio between the arc volume and the inner cathode volume. As a consequence, the fraction ratio, which can be expressed with the section ratio of the arc and the cathode, is equal to 1/16 (6.25%). The mixing temperature is calculated from the global enthalpy balance. Finally, the post-discharge is modeled by means of PFR. The model has been implemented in FORTRAN code using the PSR and SENKIN modules of the CHEMKIN II package[48].

Results and discussion

Various parameters have been studied to assess their influence on the reformer performances: O/C, input current, mass flow rate and cathode length. Unless otherwise specified, O/C is equal to 0.6 for the first operating condition and equal to 1 for the second operating condition, the input current is 0.4 A, the exhaust gas molar flow rates are 39.10^{-3} and 32.10^{-3} $mol.s^{-1}$ respectively and the cathode length is 75 mm.

Influence of O/C ratio. Figure 4 shows the results of the influence of O/C ratio in terms of conversion rate and energy efficiency for both engine operating conditions. The range of fuel flow rate is [0.02 ; 0.24 $g.s^{-1}$] for the range of O/C [0.2 ; 3.2]. The exhaust gas flow rate is held constant.

For condition 2, the Diesel fuel decomposition is higher than 80% for O/C greater than 1.3. The second operating condition (Φ = 0.32) reaches an energy efficiency of 40% against only 15% for the first one (Φ = 0.66). The strong difference in energy efficiencies is essentially due to the

oxygen rate in the gas mixture which is twice higher at low engine load and CO_2 and H_2O which are twice lower. Oxygen has the role to bring energy to the system and allows reaching higher temperatures for low engine load as shown on figure 5. In addition, at high load, an important part of calories are absorbed by CO_2 and H_2O present in high concentrations as in an EGR system. At low load, the higher the temperatures, the better the decomposition of Diesel fuel, the faster the kinetic reactions and therefore the better the energy efficiency. In both conditions, the decreasing temperatures between T3, T4 and T5 are due to thermal losses of the system.

The peak efficiencies are reached at an O/C greater than POx stoichiometry reaction (respectively for O/C equals 1.3 and 1.5 instead of O/C = 1). Firstly, temperature is one of the most important parameter. As mentioned above, reforming reactions need a lot of energy to set quickly. More oxygen is needed to activate reforming reaction and thus a higher O/C ratio. But a part of this additional oxygen forms CO_2 (cf. figure 6). The increase of H_2O mole fraction can also be inferred by the low H_2 yield shown on figure 7 (H from inlet water not taken into account). The non-homogeneity of the plasma reformer can lead to local combustion reaction which higher the temperature and leads to better performances but higher CO_2 and H_2O production.

For each O/C ratio, figure 6 also shows that, the plasma reformer promotes CO_2 production. Dry reforming reaction does not take place because a decrease of CO_2 molar fraction compared to the initial composition is not observed. Concerning steam reforming, it maybe takes place when O/C is lower than 1. Indeed, the H_2 and CO molar fractions are quite high (4 and 8% respectively) and CO_2 fraction increases. For O/C lower than 1, the high excess of fuel induces a high production of CH_4 and a very low conversion rate which can be associate with methanation. CH_4 mole

fraction must be decreased at maximum as it is a regulated pollutant. For O/C higher than 2, conditions are getting close to combustion reaction and high temperature, high CO_2 and low CH_4 production are observed.

The H_2/C ratio of Diesel fuel is equal to 0.92 and thus generally more CO than H_2 is produced. It has been proved that H_2 has a higher reduction power than CO[63,64]. But, H_2 production is more sensitive than CO to the post-discharge temperature. During transient regime, H_2 and CH_4 fractions vary inversely proportionally with the temperature.

Deposited power is represented on figure 8. The lower the oxygen rate, the higher the deposited power. In condition 2 at O/C = 1.3, 15% and 8% of dry molar fraction of CO and H_2 respectively for a deposited power of 720 W have been reached. In these conditions, the dry molar fraction of CH_4 is only 1.6%. For condition 2, the energy consumption is comprised between 4.6 and 7.7 $MJ.kg^{-1}$ of outlet syngas (H_2 + CO). Using a pulse discharge could help to decrease the energy cost of the process. The deposited are then taken as an input for models.

In this study, another important parameter to consider is the reducer molar flow rate, which determines the NOx trap regeneration duration. The figure 9 shows that the highest syngas production rate is for O/C = 0.8 for the first operating condition and O/C = 1.3 for the second one. A production of 2.10^{-3} $mol.s^{-1}$ has been reached in the first operating condition and 7.10^{-3} $mol.s^{-1}$ for the second one. The best compromise between energy efficiency, syngas molar flow rate and pollutant emissions are at O/C = 1 and O/C = 1.4 for the operating conditions 1 and 2 respectively.

The Euro V passenger car engines have to emit less than 180 $mg.km^{-1}$ of NOx, and typically their real NOx emission are close to 150 $mg.km^{-1}$ of NOx. The Euro VI regulation imposes a NOx emission lower than 80 $mg.kg^{-1}$. Consequently, 70 $mg.kg^{-1}$ of NOx have to be treated by the NOx trap. The homologation of European vehicles is based on NEDC (New European Driving Cycle) which is 11 km long. Assuming one regeneration during the cycle and that the NOx emitted are essentially NO_2, the NOx trap has to store $16.7.10^{-3}$ mol of NOx. Internal experiments in Renault showed that 5 moles of syngas are needed to reduce 1 mole of NOx. Without scaling up the mass flow rate, 7.10^{-3} $mol.s^{-1}$ of syngas leads to a NOx trap regeneration duration of 12 seconds which is a very promising. At the contrary, the first condition leads to a NOx trap regeneration duration of 45 s and is not competitive compared to catalytic processes. The catalytic reformers achieve results close to thermodynamics *i.e.* close to an energy efficiency of 70 % and a conversion rate of 100 %. In the second case, the plasma reformer achieved an energy efficiency of 40 % and a conversion rate greater than 90 %. These results are hopeful for a NTP working in a weakly oxidative environment.

Influence of input current. The monitoring of the input current directly affects the input power injected in the system. The electrical power onboard a vehicle is an expensive resource and its consumption shall be limited for post-treatment purposes. Figure 10 shows the performances of the reformer in function of input current. In the input current range [0.25; 0.6 A], the deposited power varies quasi-linearly with the current (cf. figure 11) as long as we stay in the glidarc zone. The glidarc frequency is determined by hydrodynamic parameters and cannot be varied. In NOx trap regeneration conditions, the quasi-continuous regime which gave the best results with ethanol, E85 and gasoline[4,5] cannot be reached anymore. A typical oscillogram is shown on

figure 12. The instabilities of the discharge are mainly due to reactive conditions. The stability increases with the current.

The performances at high load are quite low and even a current of 0.6 A (P = 940 W) cannot reach an adequate temperature to quicken the POx reaction. At low load, the energy efficiency grows quasi-linearly with the input current and hence with the deposited power until 0.4 A. The energy efficiency and the conversion rate reached 31% and 58% respectively for I = 0.4 A and 35% and 60% respectively for I = 0.6 A while the deposited power raises from 730 to 1180 W. Afterwards, an input current of 0.4 A is therefore considered because of onboard application which has limited usable power.

Influence of exhaust gas flow rate. One can observe in figure 13 that the higher the exhaust gas flow rate, the lower the volume power injected and the lower the performances. Figure 14 shows that the syngas molar flow rate is quasi-constant at $1.9.10^{-3}$ $mol.s^{-1}$ for the first engine condition. For the second condition, a better syngas molar flow rate is attained ($4.8.10^{-3}$ $mol.s^{-1}$) between 30.10^{-3} and 40.10^{-3} $mol.s^{-1}$ exhaust gas flow rate. This exhaust gas molar flow rate corresponds to a 3.5 - 4.5% range of total exhaust gas emitted by the engine. Figure 15 shows that post-discharge temperatures reach a maximum for both engine conditions around an exhaust gas molar flow rate of 42.10^{-3} $mol.s^{-1}$. For lower exhaust gas flow rate, the partial oxidation reaction is aided by a higher plasma power density but the low quantities of fuel and oxygen release less energy, for a similar enthalpy of reaction. For higher exhaust gas flow rate, the resident time becomes lower, the POx reaction cannot set completely and temperatures drop. A scale up of the exhaust gas flow rate was not further considered because it did not decrease the NOx trap regeneration duration.

Influence of cathode length. In order to optimize the energy cost, the arc length can be tuned by means of cathode length. The plasma reactor allows using different lengths of cylinder electrode. If the arc can reach the cathode extremity, the higher the cathode length, the higher the plasma length and the higher the voltage drop. Thus the deposited power can be increased with an input current held constant. Figure 16 shows that, even if the input power increases slightly (on average 7%), the energy efficiency and conversion rate decrease for a longer cathode. We suppose that, for a 100 mm long cathode, the arc does not reach the extremity and therefore the arc treats less gas. Previous results in POx conditions showed that a shorter cathode (50 mm long) leads also to decrease performances. For shorter cathode, the deposited power is insufficient and the reaction volume too small. The 75 mm cathode is the most adapted one regarding the energy cost and the performances.

Comparison between the 2 models and the experimental results. To investigate the highest energy efficiency which can be obtained, thermodynamics calculations have been realized. The results are shown on figure 17. The input power is not kept constant and is based on experimental results (cf. figure 8) because the deposited power varies with the operating conditions and O/C.

For both conditions, the highest energy efficiency is attained for O/C = 0.8 and the energy efficiency reaches 86 % for the first condition and 92 % for the second one. For the second condition, the highest energy efficiency is at stoichiometry of *n*-heptane with oxygen from O_2, CO_2 and H_2O. For the first condition, the maximal energy efficiency does not correspond to the stoichiometry of *n*-heptane with oxygen from O_2, CO_2 and H_2O. Figure 18 shows that, at

stoichiometry, the equilibrium temperature is too low (900 K). *n*-heptane is not completely oxidized and a high CH_4 fraction is produced.

The exhaust gas Diesel fuel reforming has also been simulated by means of a 1D model and the results have been compared to the experimental results and thermodynamics results. It can be observed, also on figure 17, an important shift in energy efficiency between experiments and 1D model. Firstly, the energy efficiency discrepancy mainly comes from thermal losses. The model assumes the adiabaticity of the medium. Secondly, the perfect and instantaneous mix at the torch exit is far removed from experimental torch exit which is highly non-homogeneous. Local non-homogeneities could also appear in the plasma reactor leading to H_2O and CO_2 production instead of H_2 and CO. However, the model trends are similar to the experimental trends. For O/C higher than 1.5, the experiments and the 1D model are very close to thermodynamics results and consequently close to the maximum achievable results. The small bump in figure 17 (right side) for O/C close to 1 is due to the consideration of real input power because it does not appear for a constant input power (not shown in this paper). In the first case, for O/C = 3.2, the experimental point is higher than thermodynamics results. This can be due either to measurement uncertainties or to a shift in O/C we have observed and seen by the efficiency peaks.

Figure 19 represents the main species along the reactor. N_2 is not represented for convenience reason. Considering only the main species, the mass balance equals 0.996 for the case represented. This figure confirms that steam reforming and dry reforming reactions are poorly involved in the exhaust gas Diesel fuel reforming process in these conditions. Indeed, comparing with the initial H_2O and CO_2 molar fractions (~ 4%), CO_2 is created along the reactor axis and a

high fraction of H_2O is produced (+ 6%) due to reactions wherein hydroxyl radicals ($OH^{\cdot}$) are involved. Hydroxyl radicals are highly reactive and promote H_2O production. This slight CO_2 production and this high H_2O production lead to decrease the syngas production and especially H_2. Nevertheless, after the reaction peak, H_2O and CO_2 rates slightly decrease to form H_2 and CO. As a consequence, water gas shift, steam and dry reforming play a minor role in the process after the reaction peak. To achieve the kinetic equilibrium, a 6 times longer adiabatic reactor is needed.

These results corroborate the experimental results which show a high conversion rate but a low H_2 yield, up to 40 % on figure 7. However, with the current state of development of our experimental test bench and associated diagnostics, it is not possible to compare the experimental reaction rates with the model. Such a comparison requires advanced diagnostic methods (intrusive and non-intrusive) such as mass spectrometry or emission optical spectroscopy.

Conclusions and Perspectives

The exhaust gas Diesel fuel reforming has been investigated using a non-thermal high voltage and low current arc plasma torch. The low O_2 availability in the plasma gas made the plasma assisted Diesel fuel reforming harder. First, it has been demonstrated that the oxygen from CO_2 and H_2O hardly ever intervene in the exhaust gas Diesel fuel reforming. At contrary, they absorb a part of calories and lower the temperature. This implies lower temperatures, lower kinetic reaction speed and lower energy efficiency compared to POx reaction. To higher the temperature, more oxygen is needed but local combustion can happen and promote H_2O and CO_2 production. A compromise has to be done between the Diesel fuel consumption, electric consumption and

methane production. At high engine load, O/C = 1 is the most suitable condition. At low engine load, an energy efficiency of 40% and a conversion rate of 95% have been reached which corresponds to a syngas dry molar fraction of 25%. For these operating conditions, a 75 mm long cathode has demonstrated the best results.

The 1D model has shown good consistency with experimental and thermodynamics trends but a shift deriving above all from the strong model hypotheses (adiabaticity and perfectly and instantaneously gas mix). In a further step, to obtain better correlations between modeling and experimental results, thermal losses and non-perfect mix will have to be taken into account together with a 2D fluid model.

The plasma torch technology for creating reducing species is a promising technology for NOx trap regeneration application which needs to be improved. Indeed, for the highest oxygen rate case, the results obtained have led to a regeneration duration of 12 s of a typical NOx trap designed to respect the Euro VI regulation. The first case, even less oxidative environment, does not seem to be competitive compared to catalytic reformer due to high regeneration duration. For this particular case, one solution could be the use of a hybrid plasma-catalysis system where the plasma will allow to decrease the catalyst volume and consequently to decrease the amount of precious metal and catalyst price. The plasma can also heat very quickly the catalyst and so get it active quicker. Plasma catalysis technology can compensate the energy cost of heat it up by another way and it allows to pre-activate the reforming reactions.

Acknowledgments

The authors gratefully acknowledge the financial and technical support of RENAULT SAS.

References

(1) Miyoshi, N.; Matsumoto, S.; Katoh, K.; Tanaka, T.; Harada, J.; Takahashi, N.; Yokota, K.; Sugiura, M.; Kasahara, K. *SAE paper 950809*. **1995**.

(2) Li, Y.; Roth, S.; Dettling, J.; Beutel, T. *Top. Catal.* **2001,** *16-17*, 139.

(3) Tsolakis, A.; Torbati, R.; Megaritis, A.; Abu-Jrai, A. *Energy Fuels* **2010,** *24*, 302-308.

(4) Abu-Jrai, A.; Rodríguez-Fernández, J.; Tsolakis, A.; Megaritis, A.; Theinnoi, K.; Cracknell, R. F.; Clark, R. H. *Fuel* **2009,** *88*, 1031-1041.

(5) Abu-Jrai, A.; Tsolakis, A. *Int. J. Hydrogen Energy* **2007,** *32*, 2073-2080.

(6) Tsolakis, A.; Megaritis, A. *Int. J. Hydrogen Energy* **2005,** *30*, 731-745.

(7) Tsolakis, A.; Hernandez, J.; Megaritis, A.; Crampton, M. *Energy Fuels* **2005,** *19*, 418-425.

(8) Yap, D.; Megaritis, A.; Wyszynski, M. *Energy Fuels* **2004,** *18*, 1315-1323.

(9) Tsolakis, A.; Megaritis, A. *Int. J. Hydrogen Energy* **2004,** *29*, 1409-1419.

(10) Tsolakis, A.; Megaritis, A.; Wyszynski, M. *Energy Fuels* **2003,** *17*, 1464-1473.

(11) Abu-Jrai, A.; Tsolakis, A.; Theinnoi, K.; Cracknell, R.; Megaritis, A.; Wyszynski, M. L.; Golunski, S. E. *Energy Fuels* **2006,** *20*, 2377-2384.

(12) Tsolakis, A.; Megaritis, A.; Wyszynski, M. *Fuel* **2004,** *83*, 1837-1845.

(13) Tsolakis, A.; Megaritis, A.; Yap, D. *Energy Fuels* **2008,** *33*, 462-470.

(14) Tsolakis, A.; Megaritis, A.; Golunski, S. *Energy Fuels* **2005,** *19*, 744-752.

(15) Abu-Jrai, A.; Tsolakis, A.; Theinnoi, K.; Megaritis, A.; Golunski, S. E. *Chem. Eng. J.* **2008,** *141,* 290.

(16) Xu, H. M.; Myszynski, M. L.; Megaritis, A.; Yap, D.; Wilson, T.; Qiao, J.; Richardson, S.; Golunski, S.; Peucheret, S. *Int. J. Engine Res.* **2007,** *8,* 29-40.

(17) Yap, D.; Peucheret, S.; Megaritis, A.; Wyszynski, M.; Xu, H. *Int. J. Hydrogen Energy* **2006,** *31,* 587-595.

(18) Tsolakis, A.; Megaritis, A. *Biomass Bioenergy* **2004,** *27,* 493-505.

(19) Abu-Jrai, A.; Tsolakis, A.; Megaritis, A. *Int. J. Hydrogen Energy* **2007,** *32,* 3565-3571.

(20) Vincent, A.; Daou, F.; Amouroux, J. *High Temp. Mater. Processes* **2002,** *6,* 167-180.

(21) Vincent, A.; Daou, F.; Santirso, E.; Moscosa, M.; Amouroux, J. *High Temp. Mater. Processes* **2003,** *7,* 267-275.

(22) Dors, M.; Mizeraczyk, J.; Czech, T.; Rea, M. *J. Electrost.* **1998,** *45,* 25-36.

(23) Filimonova, E.; Kim, Y.; Hong, S.; Song, Y. *J. Phys. D: Appl. Phys.* **2002,** *35,* 2795-2807.

(24) Mok, Y. S.; Koh, D. J.; Kim, K. T.; Nam, I.-S. *Ind. Eng. Chem. Res.* **2003,** *42,* 2960-2967.

(25) Chae, J. *J. Electrost.* **2003,** *57,* 251-262,

(26) Skalska, K.; Miller, J. S.; Ledakowicz, S. *Sci. Total Environ.* **2010,** *408,* 3976-3989.

(27) Chen, H. L.; Lee, H. M.; Chen, S. H.; Chao, Y.; Chang, M. B. *Appl. Catal., B* **2008,** *85,* 1-9.

(28) Durme, J. V.; Dewulf, J.; Leys, C.; Langenhove, H. V. *Appl. Catal., B* **2008,** *78,* 324-333.

(29) Rollier, J.-D.; Gonzalez-Aguilar, J.; Petitpas, G.; Darmon, A.; Fulcheri, L.; Metkemeijer, R. *Energy Fuels* **2008,** *22,* 556.

(30) Rollier, J.-D.; Petitpas, G.; Gonzalez-Aguilar, J.; Darmon, A.; Fulcheri, L.; Metkemeijer, R. *Energy Fuels* **2008,** *22,* 1888.

(31) Gonzalez-Aguilar, J.; Petitpas, G.; Lebouvier, A.; Rollier, J.-D.; Darmon, A.; Fulcheri, L. *Energy Fuels* **2009,** *23,* 4931.

(32) Petitpas, G.; Gonzalez-Aguilar, J.; Darmon, A.; Fulcheri, L. *Energy Fuels* **2010,** *24,* 2607,

(33) Petitpas, G.; Rollier, J.-D.; Darmon, A.; Gonzalez-Aguilar, J.; Metkemeijer, R.; Fulcheri, L. *Int. J. Hydrogen Energy* **2007,** *32,* 2848.

(34) Lee, D. H.; Kim, K. T.; Cha, M. S.; Song, Y. H. *Proc. Combust. Inst.* **2007,** *31,* 3343.

(35) Kim, S. C.; Chun. *Int. J. of Energy Res.* **2008,** *32,* 1185.

(36) Bromberg, L.; Rabinovich, A.; Alexeev, N.; Cohn, D. R., 1999, Proceedings of the 1999 U.S DOE Hydrogen Program Review, NREL/CP-570-26938.

(37) Bromberg, L.; Crane, S.; Rabinovich, A.; Kong, Y.; Cohn, D. R.; Heywood, J.; Alexeev, N.; Samokhin, A., 2003.

(38) Bromberg, L.; Cohn, D.; Hadidi, K.; Heywood, J.; Rabinovich, A., 2005, PSFC/JA-05-22.

(39) Bromberg, L.; Cohn, D.; Rabinovitch, A.; Alexeev, N.; Samokhin, A.; Hadidi, K.; Palaia, J.; Margarit-Bel, N., 2006, PSFC/JA-06-03.

(40) Crane, S.; Iverson, B.; Goldschmidt, S.; Greathouse, M.; Khadiya, N. *SAE paper 2005-01-3547,* **2005**.

(41) Li, D.; Li, X.; Bai, M.; Tao, X.; Shang, S.; Dai, X.; Yin, Y. *Int. J. Hydrogen Energy* **2009,** *34,* 308.

(42) Sugasawa, M.; Futamura, S. *IEEE Trans. Ind. Appl.* **2008,** *44,* 46.

(43) Bo, Z.; Yan, J.; Li, X.; Chi, Y.; Cen, K. *Int. J. Hydrogen Energy* **2008,** *33,* 5545.

(44) Wang, Q.; Yan, B.-H.; Jin, Y.; Cheng, Y. *Phys. Chem. Chem. Phys.* **2009,** *29,* 217.

(45) Park, C.; Kim, C.; Kim, K.; Lee, D.; Song, Y.; Moriyoshi, Y. *Int. J. Hydrogen Energy* **2010,** *35,* 1789-1796.

(46) Fulcheri, L.; Rollier, J.-D.; Gonzalez-Aguilar, J. *Plasma Sources Sci. Technol.* **2007,** *16,* 183.

(47) Santana, R. C.; Do, P. T.; Santikunaporn, M.; Alvarez, W. E.; Taylor, J. D.; Sughrue, E. L.; Resasco, D. E. *Fuel* **2006,** *85,* 643-656.

(48) Kee, R. J.; Rupley, F. M.; Miller, J. A. Sandia National Laboratories Report, SAND 89-8009, 1989.

(49) Simmie, J. *Prog. Energy Combust. Sci.* **2003,** *29,* 599.

(50) Blouch, J.; Law, C. *Proc. Combust. Inst.* **2000,** *28,* 1679-1686,

(51) Chakir, A.; Bellimam, M.; Boettner, J.; Cathonnet, M. *Int. J. Chem. Kinet.* **1992,** *24,* 385-410.

(52) Curran, H.; Gaffuri, P.; Pitz, W.; Westbrook, C. *Combust. Flame* **1998,** *114,* 149-177.

(53) Curran, H.; Gaffuri, P.; Pitz, W.; Westbrook, C. *Combust. Flame* **2002,** *129,* 253-280.

(54) Held, T.; Marchese, A.; Dryer, F. *Combust. Sci. Technol.* **1997,** *123,* 107-146.

(55) Lindstedt, R.; Maurice, L. *Combust. Sci. Technol.* **1995,** *107,* 317-353.

(56) Ranzi, E.; Gaffuri, P.; Faravelli, T.; Dagaut, P. *Combust. Flame* **1995,** *103,* 91-106.

(57) Lu, T.; Law, C. K. *Combust. Flame* **2008,** *154,* 153-163.

(58) Pedersen, T.; Brown, R. *Combust. Flame* **1993,** *94,* 433-448.

(59) Rodrigues, J. M.; Agneray, A.; Jaffrezic, X.; Bellenoue, M.; Labuda, S.; Leys, C.; Chernukho, A. P.; Migoun, A. N.; Cenian, A.; Savel'ev, A. M.; Titova, N. S.; Starik, A. M. *Plasma Sources Sci. Technol.* **2007,** *16,* 161-172,

(60) Wisman, D. L.; Marcum, S. D.; Ganguly, B. N. *J. Propul. Power* **2008,** *24,* 1079-1084.

(61) Benilov, M.; Naidis, G. *Int. J. Hydrogen Energy* **2006,** *31,* 769-774.

(62) Pateyron, B.; Delluc, G.; Calve, N. *Mécanique et Industries* **2005,** *5,* 651-654.

(63) Breen, J. P.; Rioche, C.; Burch, R.; Hardacre, C.; Meunier, F. C. *Appl. Catal., B* **2007,** *72,* 178.

(64) Takahashi, N.; Yamazaki, K.; Sobukawa, H.; Shinjoh, H. *Appl. Catal., B* **2007,** *70,* 198, Toyota.

Table 1. Main physical characteristics of Diesel fuel and *n*-heptane.

	Diesel fuel	***n*-heptane**
Empirical formula	$C_{12.31}H_{22.49}$	C_7H_{16}
Density ($g.cm^{-3}$)	0.833	0.684
Low heating value ($MJ.kg^{-1}$)	43.7	44.6
Molecular weight ($g.mol^{-1}$)	170.21	100

Table 2. Definition of both operating conditions used for calculations and experimentations.

Conditions	1 High load	2 Low load
Φ	0.66	0.32
O_2 ($\%_{mol}$)	6.8	13.9
N_2 ($\%_{mol}$)	75.8	77.4
CO_2 ($\%_{mol}$)	9.1	4.5
H_2O ($\%_{mol}$)	8.3	4.1

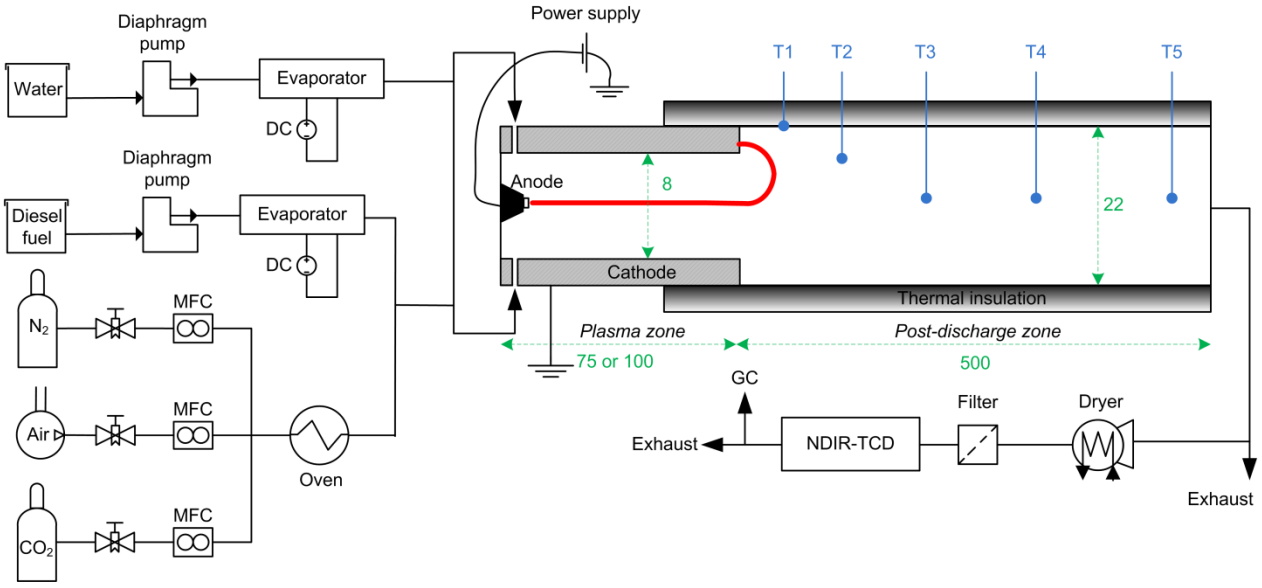

Figure 1. Schematic of the experimental set-up.

Figure 2. Photograph of the experimental bench.

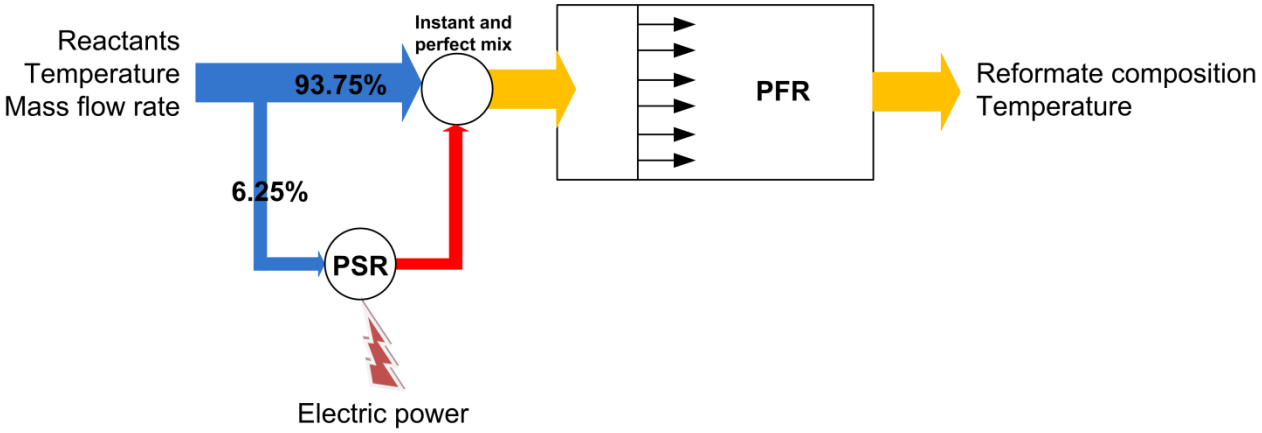

Figure 3. Diagram of the 1D multistage kinetic model describing the low current plasma reformer.

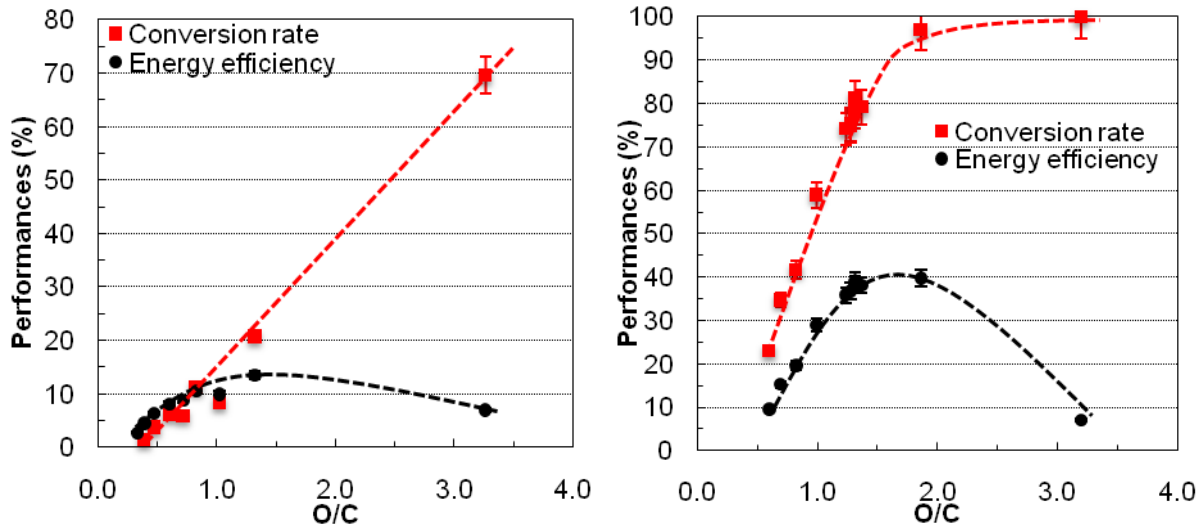

Figure 4. Experimental results of energy efficiencies and conversion rates as a function of O/C for both operating conditions. (left: condition 1; right: condition 2). I = 0.4 A.

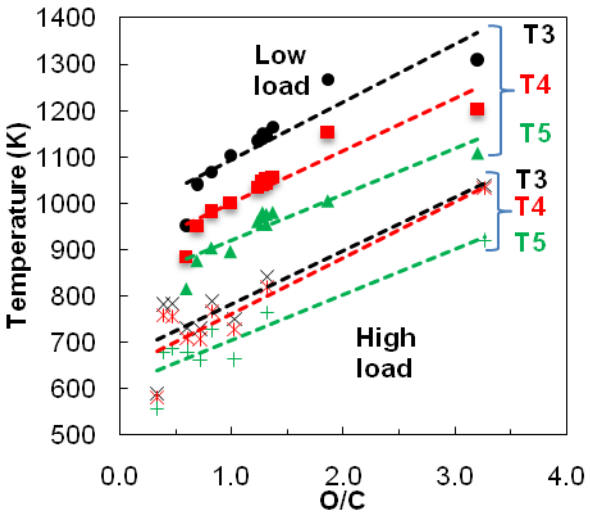

Figure 5. Temperature along the axis of the reactor.

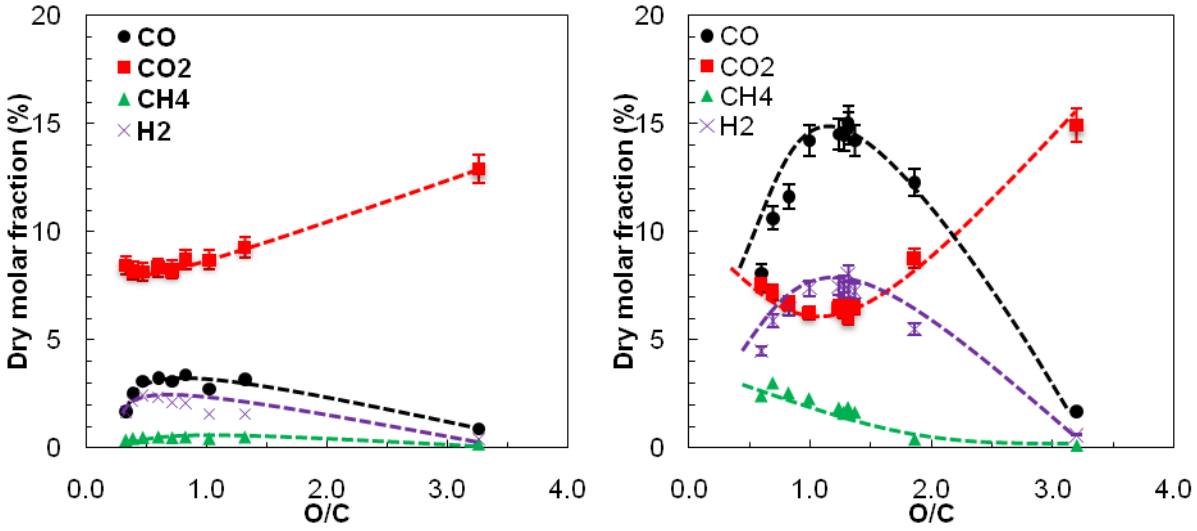

Figure 6. Dry molar fraction as a function of O/C. (left: condition 1; right: condition 2). I = 0.4 A.

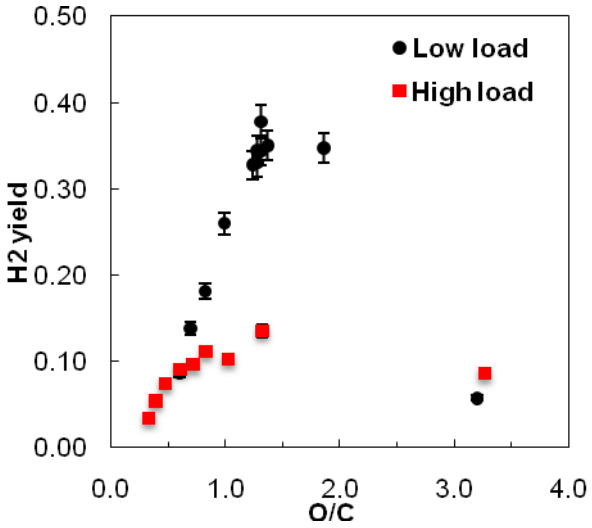

Figure 7. H_2 yield for both engine conditions.

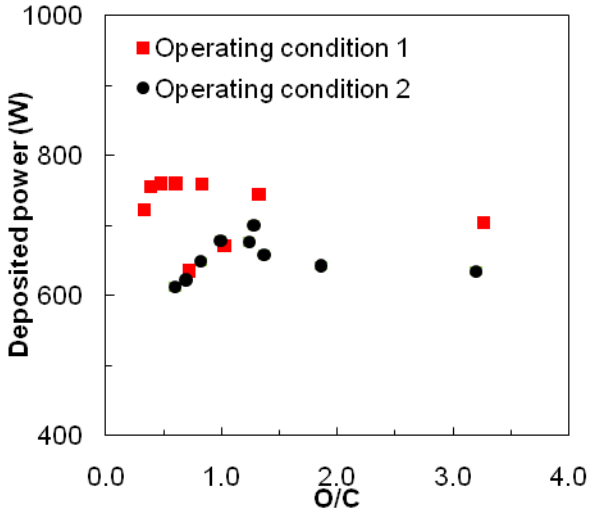

Figure 8. Deposited power into the arc discharge in function of O/C.

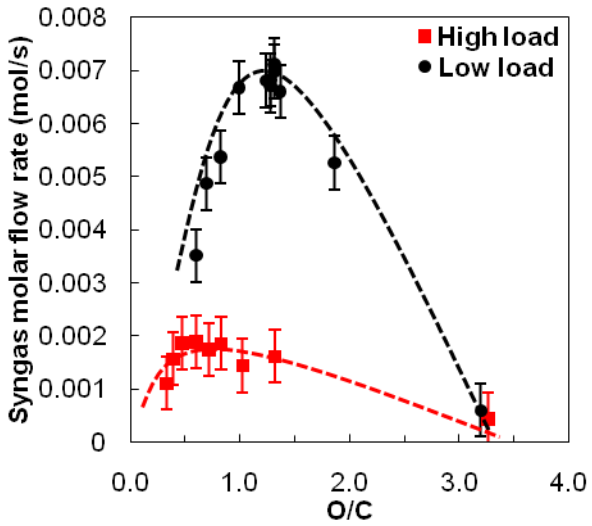

Figure 9. Experimental H_2 + CO molar flow rate as a function of O/C.

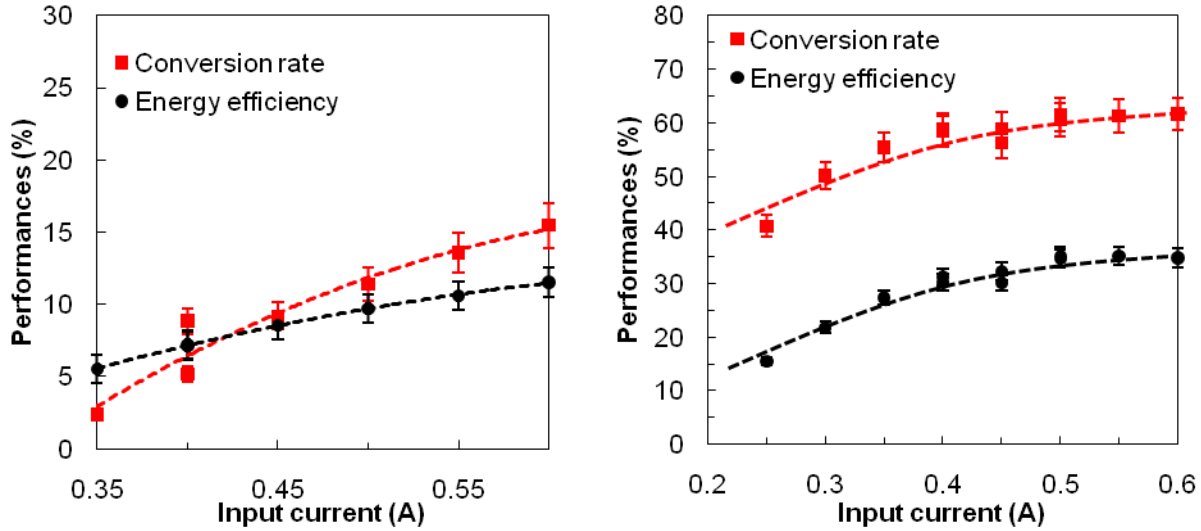

Figure 10. Performances of the plasma reformer as a function of input current for both conditions (left: condition 1, O/C = 0.6; right: condition 2, O/C = 1). Q_{fuel} = 0.13 $g.s^{-1}$.

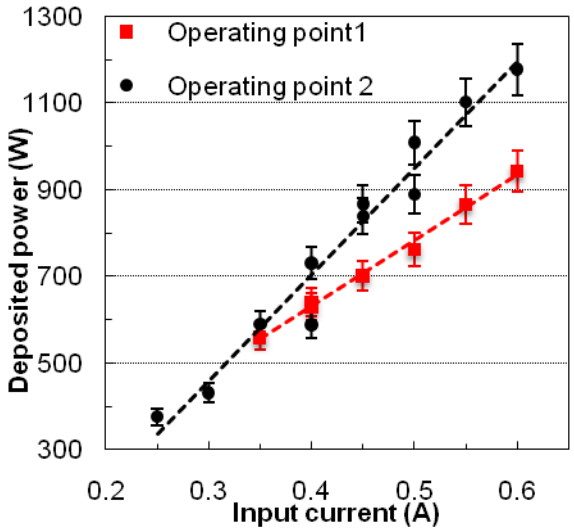

Figure 11. Deposited power as a function of input current.

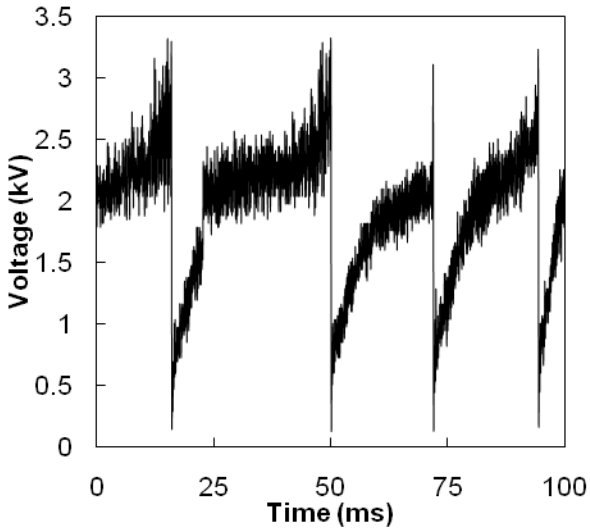

Figure 12. Typical oscillogram. Operating condition 2. I = 0.6 A.

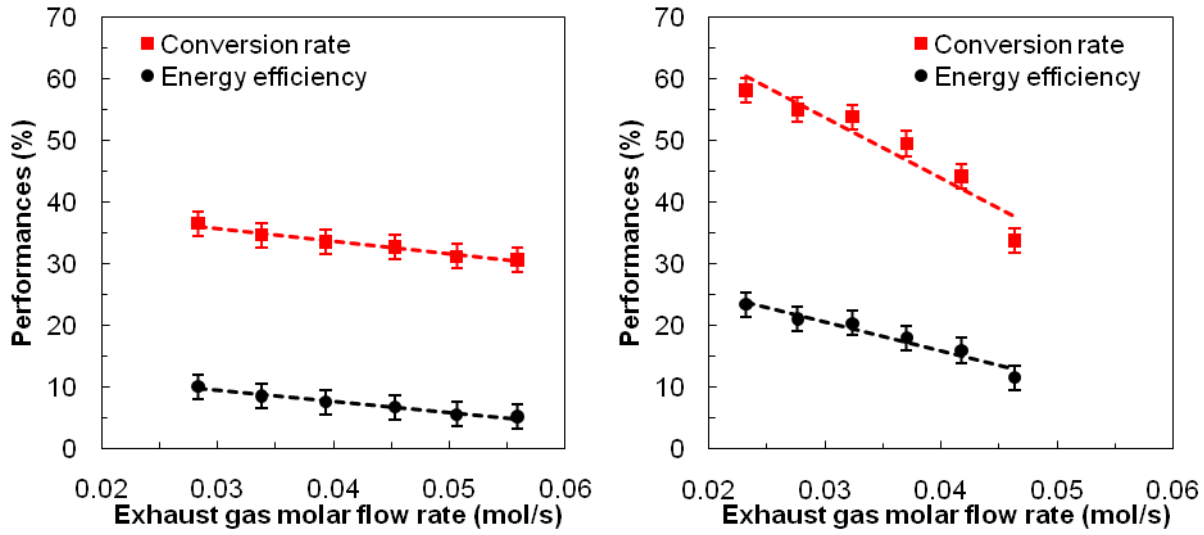

Figure 13. Performances of the plasma torch in function of exhaust gas molar flow rate. (left: high load; right: low load). I = 0.4 A. Q_{fuel} = 0.13 $g.s^{-1}$.

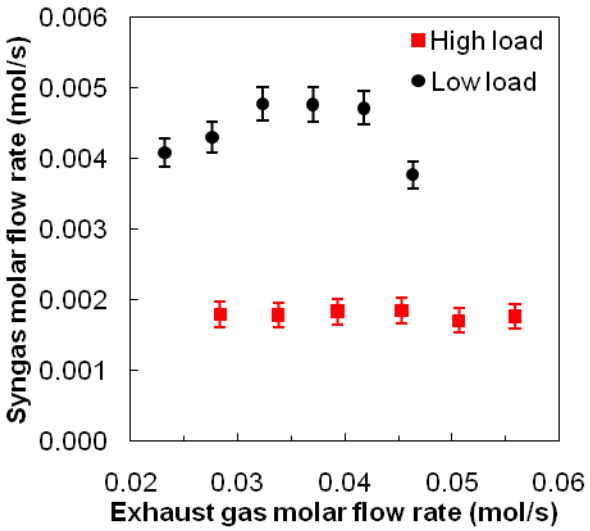

Figure 14. Syngas molar flow rate as a function of exhaust gas molar flow rate. I = 0.4 A. Q_{fuel} = 0.13 $g.s^{-1}$.

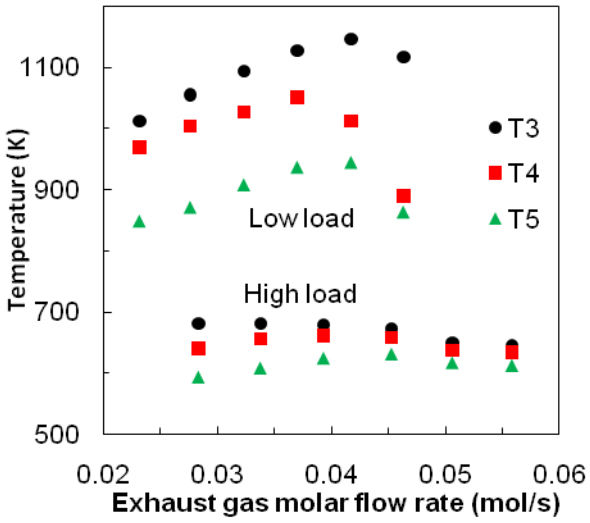

Figure 15. Temperature along the axis for both conditions. I = 0.4 A. Q_{fuel} = 0.13 $g.s^{-1}$.

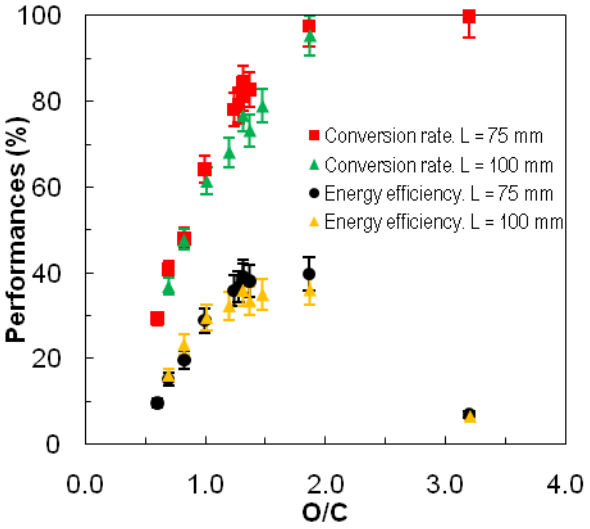

Figure 16. Experimental investigation on the influence of cathode length. Energy efficiency and conversion rate for a 75 mm and 100 mm long cathode. Operating condition 2. I = 0.4 A.

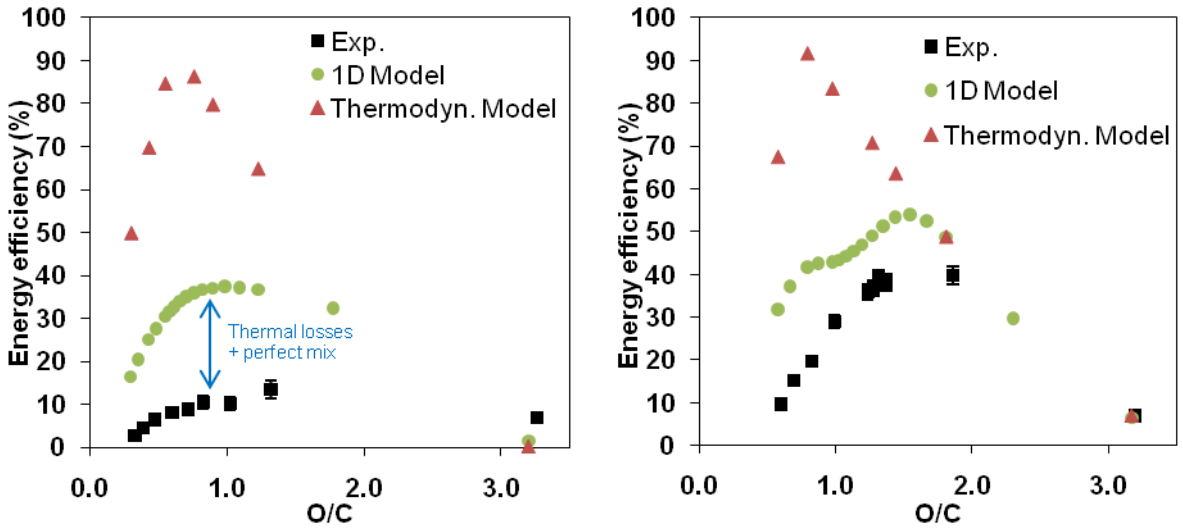

Figure 17. Exhaust gas Diesel fuel reforming: 1D model, thermodynamics model and experimental results as a function of O/C. The model used the Diesel fuel surrogate: n-heptane. 6.25% of inlet reactants pass through the plasma zone for 1D model. (left: condition 1; right: condition 2).

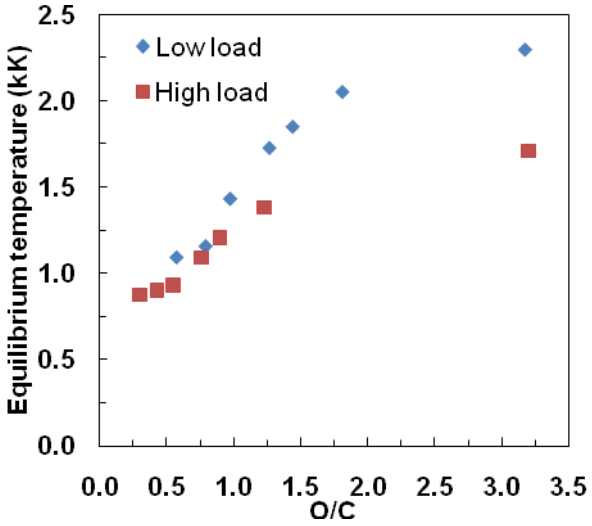

Figure 18. Equilibrium temperature from the thermodynamics model.

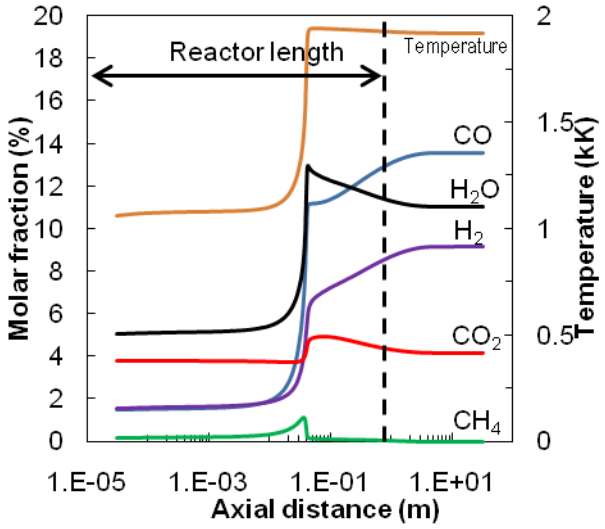

Figure 19. Main species molar fraction along the reactor. Engine condition 2. O/C = 1.54.